Thermogravimetric studies, kinetic modeling and product analysis of the pyrolysis of model polymers for technical polyurethane applications

Michael Zeller [*], Krassimir Garbev , Luca Weigel , Tilman Saatzer , Daniela Merz ,
Salar Tavakkol [*], Dieter Stapf

Institute for Technical Chemistry, Karlsruhe Institute of Technology, Hermann-von-Helmholtz-Platz 1, 76344 Eggenstein-Leopoldshafen, Germany

ABSTRACT

The pyrolysis of four kinds of common polyurethanes comprising a rigid and a flexible foam, a cast elastomer, and a thermoplastic polyurethane (TPU) was investigated by thermogravimetric analysis and pyrolysis-gas chromatography/mass spectrometry (Py-GC/MS). All samples are based on methylene diphenyl diisocyanate (MDI), with polyether polyols as the soft segment of the foams and polytetrahydrofuran as the soft segment of the cast elastomer and TPU. Each polyurethane degrades in a two-step manner with a high correlation between the polymer structure and the mass loss in each step. Two kinetic modeling approaches based on either parallel or consecutive reactions were successfully applied to describe the pyrolytic degradation. The virgin polymers and pyrolysis intermediates obtained from thermogravimetry with isothermal segments at different temperatures of 350–450 °C were investigated by ATR-FTIR. Both foams exhibit retention of feedstock nitrogen in a carbonaceous intermediate while no significant residue formation and nitrogen retention are observable for cast elastomer and TPU pyrolysis. Aromatic amines in the foam pyrolysis intermediates point to the formation of a secondary polymer originating from the urethane segments in the course of the degradation. In Py-GC/MS, the foams yield nitrogen-carrying fragments of the MDI. MDI and 1,4-butanediol are regenerated from TPU pyrolysis, indicating different degradation pathways. CE pyrolysis also releases 1,4-butanediol but no nitrogen-carrying compounds are detectable. This work demonstrates the individuality of polyurethane materials in terms of their pyrolysis behavior and released products. Potential high-value products are identified in pyrolysis at laboratory scale. The findings of this study underline the need for a comprehensive examination of polyurethane pyrolysis with differentiation of polyurethane composition and morphology to optimize technical scale polyurethane pyrolysis.

1. Introduction

In the context of the climate crisis and the finiteness of fossil resources, sustainable solutions for plastic wastes are needed [1]. While many thermoplastics are suitable for mechanical recycling, a more diffuse picture emerges for thermoset plastics such as polyurethanes (PUR) and complex, partially inseparable mixed plastic wastes [2]. PUR represent approximately 5.5% of global plastics production [3]. They are synthesized from polyisocyanates and polyhydric alcohols, which form the eponymous urethane bonds by a polyaddition reaction [4]. The use of various isocyanates and polyols, as well as additives such as foaming agents, enables a wide variety of PUR with versatile properties. Typical applications include insulation materials (rigid foams), flexible foams e.g. in mattresses and upholstery as well as cast elastomers, and

thermoplastic polyurethanes for various industrial and end consumer products. Due to the comparatively complex chemistry of PUR, established recycling routes are only suitable to a limited extent. Mechanical recycling is often limited to grinding and rebonding, effectively downcycling the material [5,6]. Solvolysis aims to depolymerize and recover products of high value, e.g. polyols, or isocyanate precursors. It is a potential option for the recycling of single-variety PUR, such as soft and rigid foams, but has proven to react pronely to contaminations and is difficult to operate economically [6]. Given the limited suitability of mechanical recycling and solvolysis for PUR, pyrolysis comes into question as a robust recycling process. In pyrolysis, the goal is to convert otherwise unrecyclable and often mixed wastes to products that can substitute fossil feedstocks in the chemical industry. While the applicability of pyrolysis for complex mixed plastic wastes has been proven, it

---

was also shown that further treatment is necessary to remove heteroatoms and condition the pyrolysis products for high-value applications [7–9]. As carriers of significant amounts of nitrogen and oxygen, PUR are challenging pyrolysis feedstocks in this respect.

Numerous investigations on pyrolytic PUR degradation mechanisms and products are reported in the literature. It is generally accepted that PUR pyrolysis proceeds in two stages. In the first decomposition stage in the range of lower temperatures, the urethane bonds decompose in two competing mechanisms. Depending on the temperature and the polymer composition, either depolymerization via 4-membered ring transfer resulting in the formation of an isocyanate group and an alcohol group, or the formation of an amine and release of carbon dioxide via 6-membered ring transfer is favored. In the second decomposition stage, the polyol and secondary polymeric structures formed during the initial degradation step pyrolyze and form various products carrying nitrogen and oxygen. Available investigations often cover a specific type of PUR waste, e.g. foams [10–13], elastomers [14,15], or lab-prepared samples designed for targeted research questions [16–18].

Comparative considerations and an overall view of the pyrolysis of various PUR plastics have already been presented in several reviews [19–22]. However, a clear understanding of the pyrolysis process and critical process parameters is still missing [20]. In light of the large variety of PUR, analytical methods, and equipment, reasonable care must be taken when comparing results. In particular, the transfer and comparison of kinetic parameters are impacted in this regard [23]. Tang et al. [14] demonstrate the great benefit of combined analytical methods for the evaluation of the thermal degradation of PUR and other complex materials. Numerous recent studies dealing with polymer wastes and waste mixtures substantiate this [24–28]. In the presented study, key PUR compositions and morphologies are investigated with the aim of better understanding and mathematically describing their specific thermal degradation while maintaining comparability based on uniform analytical methods. Time- and temperature-resolved pyrolytic decomposition is observed by thermogravimetry and kinetic parameters are derived. Segmented thermogravimetric analysis provides access to non-volatile pyrolysis intermediates and approximates process conditions of technical pyrolysis processes. Py-GC/MS analyses complement this with qualitative information on the volatile pyrolysis products on a laboratory scale.

2. Material and Methods

2.1. Polymer Samples

Four model PUR representing rigid foam (RPUF), flexible foam (FPUF), cast elastomer (CE), and thermoplastic polyurethane (TPU) were selected for this study as they represent four different structural PUR applications. Coatings and adhesives, while important applications of PUR, were not considered since they typically occur in close association with other materials, rendering them less relevant for pyrolysis. Methylene diphenyl diisocyanate (MDI) was chosen as a universal isocyanate basis. The compositions of CE, RPUF, and FPUF are given in Table 1. The use of additives was avoided as far as possible to be able to attribute observed effects exclusively to the thermal decomposition of the PUR. To achieve the desired properties, the use of catalysts could not be completely avoided.

The TPU investigated in this study is comprised of polytetrahydrofuran (PTHF), 1,4-butanediol (1,4-BDO), and MDI with small amounts of dibutylhydroxytoluene-based antioxidant. It is commercially available, so the exact composition is not disclosed. Elemental Analyses were performed in a Leco TruSpec Micro. The results are displayed in Table 2.

Table 1
Composition of model PUR investigated in the presented study.

Ingredient	Rigid Foam	Flexible Foam	Cast Elastomer
	Wt.-%	Wt.-%	Wt.-%
Polytetrahydrofuran	-	-	77.6
Propylene oxide-based Polyetherols	31.7	56.1	-
Ethylene oxide-based Polyetherols	-	10.3	-
Sorbitol	7.2	-	-
Glycerine	4.1	1.6	-
MDI	56.3[1,2]	28.8[1,2]	20.3[1]
1,4-Butanediol	-	-	2.0
Sum[3]	99.3	96.8	99.9

1 the exact isomer composition is unknown
2 sum of MDI and polymeric MDI
3 difference to 100% includes undisclosed additives and foaming agent water

Table 2
Elemental composition of model PUR investigated in the presented study.

Sample	C	H	N	O (Difference)
	Wt.-%	Wt.-%	Wt.-%	Wt.-%
Rigid Foam	70.0	6.7	6.9	16.3
Flexible Foam	68.1	8.5	3.3	20.1
Cast Elastomer	70.5	9.4	2.1	17.9
Thermoplastic Polyurethane	71.5	8.4	3.7	16.3

2.2. Experimental Setups

2.2.1. Thermogravimetry

Thermogravimetric analyses (TGA) were performed using a Netzsch TG 209 F1 Libra with an automatic sample changer. The default sample size was 10 mg ± 2% weighed in corundum crucibles without a lid. Dynamic runs were carried out with heating rates from 2 K/min to 30 K/min from 30 °C to 900 °C in a nitrogen atmosphere with a total flow of approximately 60 ml/min. At the end of each experiment, the atmosphere was switched to synthetic air to oxidize residues and pyrolysis product deposits in the crucibles and the oven chamber. Experiments with isothermal segments were conducted with a constant heating rate of 5 K/min to either 350 °C, 400 °C, or 450 °C. The targeted isothermal temperature was held for 4 h. Subsequently it was heated up further to 900 °C. For detailed chemical investigation, experimental runs were terminated after the isothermal period to recover the pyrolysis intermediates. For these experiments, higher sample masses of up to approx. 35 mg were used per experiment. Each experimental setting was carried out at least twice to ensure the validity and reproducibility of the results.

2.2.2. Pyrolysis-Gas Chromatography-Mass Spectrometry

A CDS Pyroprobe 6200 DISC micropyrolyzer coupled to an Agilent 7890B Gas Chromatograph (GC) and an Agilent 5977B Mass spectrometer (MS) was employed to conduct isothermal Pyrolysis-GC/MS experiments. The micropyrolyzer is equipped with a quartz glass pyrolysis chamber wrapped by a resistively heated platinum filament, allowing precise temperature control and heating rates of several 100 °C /s. The plastic samples introduced into the pyrolysis chamber were hence pyrolyzed at quasi-isothermal conditions. The sample size was approximately 50 μg for all conducted experiments. Pyrolysis experiments were carried out at temperatures of 600 °C for one minute. The internal piping and the transfer line to the GC/MS were heated to 350 °C to minimize condensation of high boiling products.

The released pyrolysis products were swept to the GC by a helium gas flow and separated by a Restek RXI-5MS column (30 m, 0.25 mm inner diameter, 1.0 μm film thickness). The GC inlet was set to the maximum temperature of 300 °C in split mode with a split of 100:1. A constant pressure of 70 kPa was applied. The GC oven temperature was initially

held at 35 °C for 15 min and subsequently ramped up to 120 °C at a rate of 1 °C/min followed by a second temperature ramp to 280 °C at 2.5 °C/min with a final holding time of 16 min. The MS was operated in scan mode in the range from 10 to 600 m/z with a step size of 0.1 m/z and a cycle time of 210.15 ms.

2.2.3. ATR-FTIR

ATR-IR measurements were performed on a Bruker Optics Tensor II spectrometer equipped with a deuterated triglycine sulfate (DTGS) detector and a Golden Gate ATR cell with a diamond crystal (Specac LTD, Orpington, UK). Spectra were acquired in the range 400–4000 cm^{-1} with 64 scans and a spectral resolution of 2 cm^{-1}. OPUS 8 software was used for the acquisition and evaluation of the IR spectra.

2.3. Kinetic Modeling

Dynamic TGA runs with and without isothermal segments with heating rates from 2 K/min to 30 K/min were considered for the fitting of the model parameters of PUR mass degradation. Data preparation was performed as recommended [29].

Two models from the literature were adapted for this work. Both have proven to be suitable for the modeling of the multi-staged pyrolysis process that is typical for PUR. The model used by Jomaa et al. [30] employs multiple independent parallel reactions, while Garrido et al. [10,11] assume two consecutive reactions, with the rate of the second degradation reaction influenced by the progress of the initial degradation. Since this model assumes consecutive reactions, it represents the generally accepted degradation mechanisms of PUR more precisely but is difficult to adapt for the kinetic modeling of the pyrolysis of plastic mixtures, where interactions between the polymers are possible, but do not necessarily take place. An approach based on independent parallel reactions has proven to be suitable for such complex materials [31].

The models and the parameter fitting procedures were adapted from the literature with minor changes.

Both models are based on kinetic equations using an Arrhenius approach to describe the yield α_i in dependency of the time t. Fitting parameters of the kinetic equations are the preexponential factor $k_{0,i}$ and the activation energy $E_{A,i}$. The kinetic model $f(\alpha_i)$ is dependent on the chosen approach. R and T refer to the universal gas constant and the temperature respectively.

$$\frac{d\alpha_i}{dt} = k_{0,i} \cdot \exp\left(-\frac{E_{A,i}}{R \cdot T}\right) \cdot f(\alpha_i) \tag{1}$$

2.3.1. Independent parallel reactions approach

The independent parallel reactions model (IPRM) approach uses a kinetic model $f(\alpha)$ commonly used for plastics pyrolysis according to Eq. (2).

$$f(\alpha_i) = (1 - \alpha_i)^{n_i} \tag{2}$$

Here, n_i is the order of reaction. The volatile yield α at time t is defined as follows:

$$\alpha(t) = \frac{m_0 - m(t)}{m_0 - m_\infty} \tag{3}$$

The masses m_0 and m_∞ are the initial sample mass and the sample mass at the end of the experiment, respectively.

A linear combination of multiple kinetic equations is used to calculate the total volatile yield. Per reaction a proportion parameter q_i is fitted, which determines the proportion of the yield generated in the respective reaction to the total yield. The number of parallel reactions can be chosen freely, giving the model high flexibility.

$$\frac{d\alpha}{dt} = \sum_{i=1}^{\eta} q_i \cdot \frac{d\alpha_i}{dt} \tag{4}$$

$$\sum_{i=1}^{\eta} q_i = 1 \tag{5}$$

Per employed reaction a pre-exponential factor $k_{0,i}$, an activation energy $E_{A,i}$, an order of reaction n_i, and a proportion parameter q_i are fitted. For η parallel reactions, this results in a total of $4 \cdot \eta$ model parameters, which are bundled in the vector a.

$$a = [q_1, ..., q_\eta, E_{A,1}, ..., E_{A,\eta}, k_{0,1}, ..., k_{0,\eta}, n_1, ..., n_\eta] \tag{6}$$

For the parameter optimization, the *patternsearch* algorithm in MATLAB [32] was used to find the minimum of the optimization function shown in Eq. (9). The variables N_{TGA} and $N_{exp,l}$ in Eqs. (7) and (8) describe the number of TG experiments and the number of data points contained therein. The least-square errors of the measurement curves are each normalized to the number of data points as well as the square of the maximum conversion rate. The parameter λ allows a weighting of the optimization function with respect to integral and differential curve fits. It creates flexibility and adaptability to a wider range of plastics and can also be used as an optimization parameter [30].

$$OF_{int}(a) = \sqrt{\sum_{l=1}^{N_{TGA}} \sum_{z=1}^{N_{exp,l}} \frac{\left[\alpha_{M,exp,l}(t_z) - \alpha_{M,cal,l}(t_z, T_z, a)\right]^2}{N_{exp,l}}} \tag{7}$$

$$OF_{diff}(a) = \sqrt{\sum_{l=1}^{N_{TGA}} \sum_{z=1}^{N_{exp,l}} \frac{\left[\frac{d\alpha_{M,exp,l}(t_z)}{dt} - \frac{d\alpha_{M,cal,l}(t_z, T_z, a)}{dt}\right]^2}{N_{exp,l} \cdot \left.\frac{d\alpha_M(t_z)}{dt}\right|_{max}^2}} \tag{8}$$

$$OF(a) = 100 \cdot \sqrt{(1-\lambda)OF_{diff}^2 + \lambda OF_{int}^2} \quad \lambda \in [0,1] \tag{9}$$

In test runs, the best results were obtained with an equal distribution of differential and integral proportions, so that λ was fixed at 0.5. The starting values of the optimization were determined using the Friedman method [33].

2.3.2. Consecutive reactions approach

The consecutive reactions model (CRM) used in this work is fixed to two steps, with the kinetics of the second reaction being dependent on the first step. The kinetic model of the first reaction is equivalent to Eq. (2), although using a different definition of α, as described in Eq. (10).

$$\alpha_i(t) = \frac{v_i(t)}{v_{i,\infty}} \tag{10}$$

Here, v_i is the amount of volatiles released in the respective degradation step at time t, while $v_{i,\infty}$ is the maximum volatile amount, that is released per step. Hence, for $v_{1,\infty}$ this value ranges from 0 to 1 and for $v_{2,\infty}$ from 0 to $(1-v_{1,\infty})$. These variables are subject to the optimization performed to obtain the kinetic parameters. The parameters to be optimized are bundled in vector b.

$$b = [v_{1,\infty}, v_{2,\infty}, E_{A,1}, E_{A,2}, k_{0,1}, k_{0,2}, n_1, n_2] \tag{11}$$

The volatile release of reaction 2 depends on the yield of reaction 1, resulting in the kinetic model Eq. (12).

$$f(\alpha_2) = (\alpha_1 - \alpha_2)^n \tag{12}$$

The normalized sample mass m_{cal} at time t, which gives the amount of volatiles released in pyrolysis is thus expressed by Eq. (13).

$$m_{cal}(t) = 1 - v_{total} = 1 - (\alpha_1 v_{1,\infty} + \alpha_2 v_{2,\infty}) \tag{13}$$

The optimization function used for parameter fitting is:

$$OF(b) = \sum_{l=1}^{N_{TGA}} \sum_{z=1}^{N_{exp,l}} \left[m_{exp,l}(t_z) - m_{cal,l}(t_z, b)\right]^2 \tag{14}$$

MATLAB algorithms *MultiStart* and *GlobalSearch* [32] were employed for the optimization.

3. Results & Discussion

3.1. Dynamic Thermogravimetry

Fig. 1 gives the mass loss curves (left) and their derivatives (right) of the four model PUR at a heating rate of 10 K/min. The plastics differ significantly in the mass loss observed in the respective decomposition stages and the amount of formed residue.

The rigid PUR foam decomposes in a pronounced first stage beginning at roughly 250 °C with a peak at approx. 340 °C and a mass loss of approx. 62% until approx. 420 °C. The peak of the secondary decomposition is at approx. 480 °C with a further mass loss of about 22% until the maximum conversion is reached at ca. 550 °C. The residual mass fraction at 900 °C is about 14%. In contrast, the initial decomposition in the FPUF is low at about 11% and blurs with the secondary decomposition stage in the temperature window from 220 °C to about 450 °C. A residual amount of approx. 6% remains. More distinct decomposition ranges are observed for the PTHF-based CE and TPU. CE releases 28% and 70% volatiles in its decomposition stages at peak temperatures of 363 °C and 418 °C, respectively. No significant residue remains. TPU decomposes with an initial mass loss of 54% up to approx. 390 °C and a secondary mass loss of 45% from 390 °C onwards, without the formation of a significant residue. Based on the thermoplastic properties of the material, it can be assumed that a high proportion of long-chain polyols is contained and that the chains are only sparingly crosslinked. The lower proportion of MDI is also expressed in the elemental composition (Table 2). Short-chain polyols and a high isocyanate content (see Table 1) were used for the synthesis of the RPUF. The proportion of urethane bonds in the polymer is thus high, which explains the intense initial decomposition stage and the increased tendency to form a residue. Since lower mass fractions of MDI and longer-chain polyols were used for the synthesis of the FPUF, the observed decomposition behavior is conclusive. Although the MDI content of CE at 20% (Table 1) is still somewhat lower than for the FPUF, the mass loss in the first decomposition stage is greater, which may be due to the added volatile 1,4-BDO, which is released during depolymerization and evaporates.

Since very little residue is formed in CE and TPU pyrolysis, it can be assumed that, in addition to the 1,4-BDO, the nitrogen-carrying products of the urethane decomposition also evaporate. The absence of a foaming agent in the CE and TPU formulation prevents the formation of nitrogen-containing bonds other than urethane during synthesis and thus alters the pyrolytic degradation behavior. The strong mass loss in the first stage of TPU pyrolysis can be explained, as in the case of the CE, by the release of the chain extender 1,4-BDO and the urethane pyrolyzates.

3.2. Segmented Thermogravimetry & Intermediate Analysis

Experiments with isothermal segments, shown in Fig. 2, reveal that in the low-temperature range, only incomplete conversion of the PUR can be achieved. At an isothermal temperature of 350 °C, which in the case of RPUF is in the range of the peak of the first decomposition step, almost no mass loss is noticeable after 4 h for RPUF. The residual mass at the end of the isothermal period is about 33%. It can be assumed that the decomposition of the polyol components of the PUR already takes place at 350 °C, but only comparatively slowly, and long-chain secondary polymers are formed as decomposition products. These evaporate only with difficulty, which is why only a slow decrease in mass can be observed. At isothermal temperatures of 400 °C and 450 °C, approx. 21% and 17% of the original sample mass remain after 4 h, respectively. At these two isothermal temperatures, the decomposition range of the urethane bonds is crossed, which is why a rapid decomposition of these bonds with a superimposed decomposition of the soft segment can be assumed here. Due to the elevated temperature, the rate of decomposition of the urethane and polyol bonds is increased. The higher temperature facilitates the evaporation of the pyrolysis products, as evidenced by the more rapid mass loss. Almost complete conversion is achieved.

The residual mass at 900 °C is not significantly affected by the isothermal pyrolysis at the holding points studied. The selected isothermal phases in the pyrolysis thus do not appear to have any influence on the amount and mechanisms of the residue formed. Several authors report an influence of the pyrolyzate evaporation and secondary reactions on the product spectrum and thus the residue formation [13, 34,35]. In the isothermal experiments performed in this work, no such effects are registered. Samples of the resulting pyrolysis intermediates were obtained from experiments terminated after the end of the isothermal phase and were analyzed with respect to their structure and elemental composition. After cooling, the intermediates present themselves as a black, brittle, partially blistered structure similarly observed by Kumagai et al. [16]. Thus, a softening or melting process of the per se thermoset polymers must have taken place.

Fig. 3 shows the IR spectra of the virgin polymers. The spectrum of the RPUF is dominated by the bands at 1222, 1511, and 1708 cm^{-1}, which are assigned to the vibrations of the urethane group. Their different intensities point to an increasing number of urethane groups in the row FPUF < CE < TPU < RPUF. The band at 1222 cm^{-1} could be attributed to asymmetrical stretching of N-CO-O [18,36] but also can be strongly influenced by (O=)C–O–C stretching mode [37–39]. The band at 1708 cm^{-1} is due to the stretching mode of C=O of the carbonyl urethane group [38] and is a product of the polymerization of isocyanate with a polyol. The broadening towards lower frequencies points to a strong influence of hydrogen bonding confirmed by the higher intensity of the ν_s N-H stretching band at 3302 cm^{-1} [40,41]. Whereas this band is very broad in the spectrum of RPUF, the spectra of the other three samples show two differentiated bands: one at 1700–1710 cm^{-1} and the second at 1730 cm^{-1} as observed in [41]. Correspondingly, the N-H modes in these samples are observed at lower frequencies (3300–3340 cm^{-1}) than that of RPUF (3300–3380 cm^{-1}) [42]. TPU shows the strongest H bonding with a very intense 1700 cm^{-1} band. The bands in the range 1500–1540 cm^{-1} are due on one hand to skeleton C-C stretching within the benzene ring [18,36], but also to in-plane bending of N-H, leading to substantial broadening towards higher wavenumbers. Generally, two bands could be resolved at about 1510 cm^{-1} and 1530 cm^{-1}, respectively, which are with different intensity ratios in the four samples. The most intense band are observed in the spectra of RPUF (1511 cm^{-1}) and TPU (1529 cm^{-1}) implying the greatest number of urethane groups in these samples. Additional ring opening vibrations give rise to bands at 1412 cm^{-1} (ν C-C) and 1595–1610 cm^{-1} (ν C=O) possibly split by Fermi resonance [43]. In the range of 1000–1120 cm^{-1} intensive composite bands assigned to ν_{as} C-O-C vibrational modes are observed. RPUF shows bands at 1074 cm^{-1} with shoulders at 1044 cm^{-1} and 1100 cm^{-1}. The soft segments of FPUF show a spectrum very similar to that of polypropylene glycol (Spectrum Nr. 25322–69–4 FDM ATR polymer database) with a very strong band at 1094 cm^{-1}. Therefore, the FPUF sample consists of a significantly lower number of urethane groups and correspondingly longer chainlike structures typical for the soft segment. The corresponding C-O-C stretching bands in the spectra of CE and TPU are positioned at about 1102 cm^{-1} with a shoulder at 1063^{-1} (CE) and 1105 cm^{-1}, 1076, and 1068 cm^{-1}(TPU). Several C-N(C) vibrations give rise to bands with middle intensity at 766, 815, and 845 cm^{-1} (ν_s C-N and C-N-C). Corresponding ν_{as} C-N-C is observed at 1156 cm^{-1}. Coupled bending N-C-O and CH$_2$ are observed at 1308–1310 cm^{-1} [38]. Stretching vibrations of C-H in methylene and methyl groups are observed at 2872, 2904, and 2930 cm^{-1}(ν_s modes) and at 2977 cm^{-1} (ν_3 modes) in the spectra of RPUF and FPUF. Corresponding bending modes are observed as bands at 1018 cm^{-1} (in-plane δ C-H), at 1375 cm^{-1} (δ_s CH$_3$), and at 1453 cm^{-1} (δ_{as} CH$_3$) probably mixed with (δ_s CH$_2$). The C-H stretching region shows quite similar bands in the spectra of TPU and CE. They are at considerably lower frequencies 2800 cm^{-1}, 2856–2860 cm^{-1} (most intense band), 2920 cm^{-1}, and 2940 cm^{-1} than those of the RPUF and FPUF.

All bands in connection with C-N, N-H, C=O, and C-C vibrations of the benzene rings are with significantly lower intensity in the spectrum
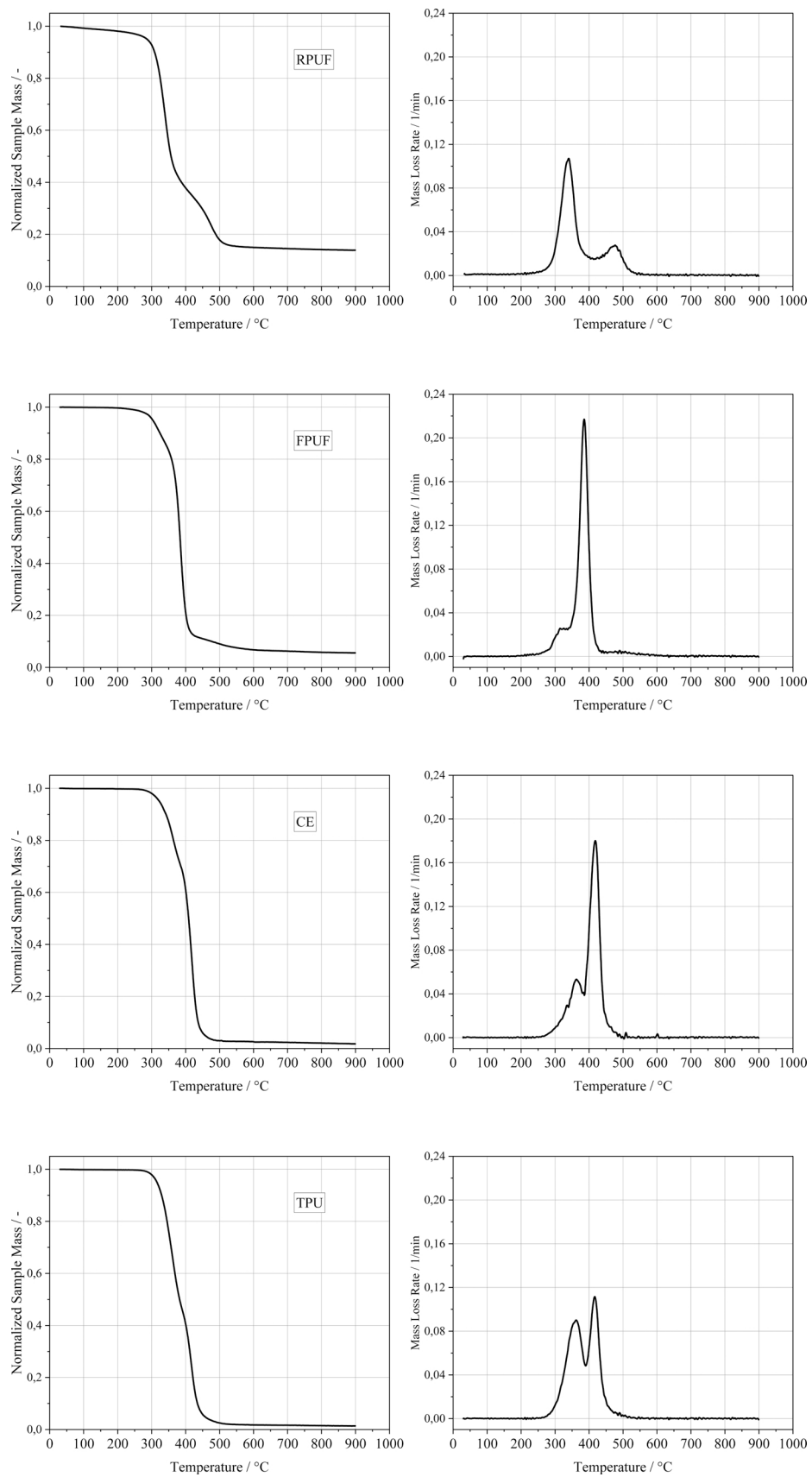
Fig. 1. Mass loss curves (left) and derivatives (right) of model PUR in dynamic pyrolysis experiments with a heating rate of 10 K/min.
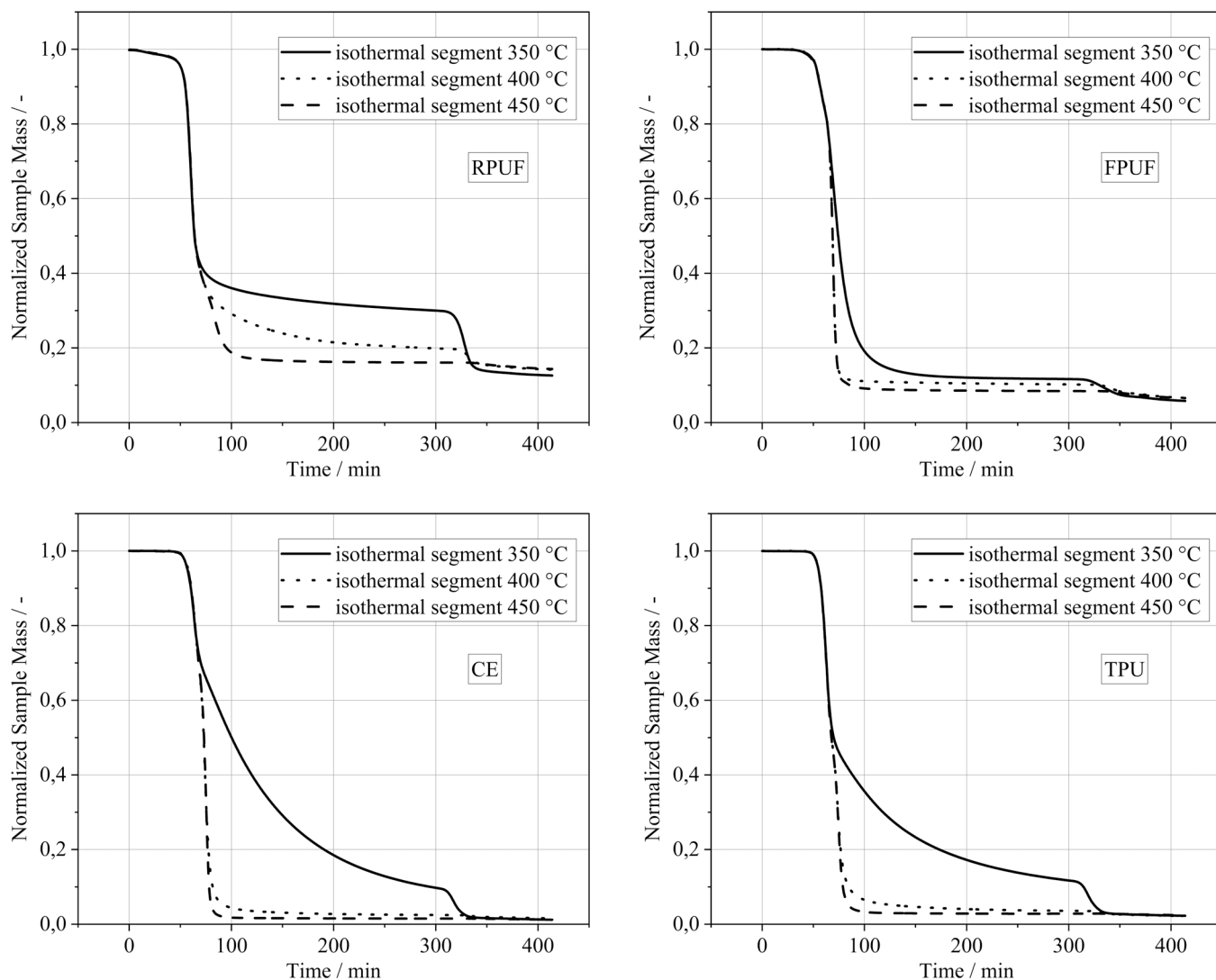
Fig. 2. Thermogravimetric Mass Loss of RPUF (top left), FPUF (top right), CE (bottom left), and TPU (bottom right) in segmented experiments with 5 K/min dynamic heating rate and 4 h isothermal holding time at different temperatures.

of the FPUF sample. None of the samples show N-C-O bands in the range 2100–2300 cm^{-1} typical for MDI leading to the conclusion that the educts are fully reacted.

The IR spectra of the pyrolysis intermediates show significant differences from that of the virgin RPUF (Fig. 4). The spectra of the samples pyrolyzed at 400 °C and 450 °C are very similar, pointing to the almost identical conversion at these temperatures with the isothermal time of 4 h. The most significant changes in the spectrum of the 350 °C include a complete drop of the intensity of the carbonyl urethane group band at 1708 cm^{-1} (ν C=O), 2) and disappearance of the C-O-C stretching bands in the range 1040–1150 cm^{-1} pointing to the disintegration of the soft segments (polyols). The band at 1308 cm^{-1} assigned to coupled bending of N-C-O and CH$_2$ also loses intensity. Therefore, the first stage of the PUR degradation is a reverse polyaddition with subsequent formation of alcohol and isocyanate groups [44]. The N=C=O bands typical for isocyanate at 2100, 2280 cm^{-1} are not observed because monomeric isocyanate either evaporates [45] or undergoes secondary reactions. The breakdown of the carbamate group begins already at 200 °C [36]. Bands typical for C-N and C-N-C vibrations (768 cm^{-1} and 815 cm^{-1}, respectively) are on the contrary persistent and are seen even after 450 °C. The bands typical for C-C and C=C stretching of the benzene rings (1412, 1510, and 1600 cm^{-1}) show similar behavior, being the most intense peaks in the intermediate products after 400 and 450 °C. This

observation is consistent with the accumulation of aromatic structures as a result of the depolymerization and volatilization of the soft segments [15]. The spectrum of the 350 °C sample shows striking similarities with 4,4′-MDA (Spectrum Nr. 101–77–9 FDM database). Especially the CH$_2$ and N-H stretching bands in the range 2800–3100 and 3100–3500 cm^{-1}, respectively, show almost identical frequencies with these of MDA. The band at 1177 cm^{-1}, assigned to the C-N stretching mode of the 4,4′-MDA, seems to lose intensity upon increasing the temperature of treatment. Similar behavior shows the band at 1270 cm^{-1}. Therefore, at least a partial disintegration of the 4,4′-MDA to polyaromatic char residue takes place.

The broad band at about 1600 cm^{-1} could be additionally influenced by bending mode vibrations of type N-H typical for amines as probable derivates of isocyanate [46]. A comparison with the FDM database confirmed the similarity of the 400 and 450 °C spectra with N-dimethylbenzenamine. The band at 1510 cm^{-1} could be influenced by d N-H and v C-N modes [38]. It is smeared in the 450 °C spectrum, which implies partial decomposition of urethane groups during pyrolysis. The in–plane bending δ-CH (1017 cm^{-1}) and δ CH$_3$ (1376 cm^{-1}) bands are also clearly seen in these spectra.

The occurrence of the band at 3630 cm^{-1} in all intermediate products is interesting. It could be unambiguously assigned to OH stretching mode and points to alcohol as a natural product of the depolymerization
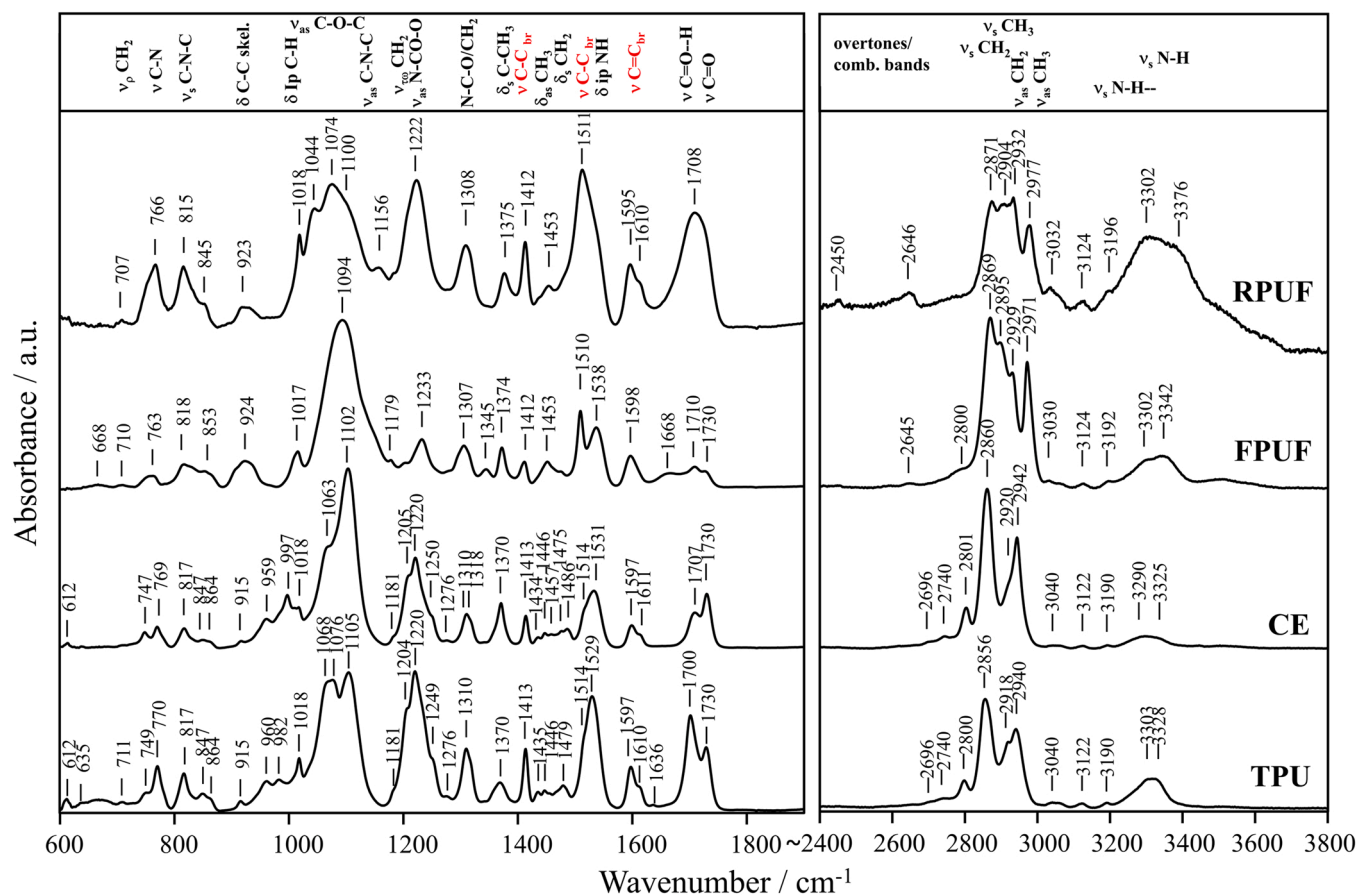
Fig. 3. ATR-FTIR Spectra of virgin polymers in the ranges 800–1900 cm^{-1} (left) and 2400–3800 cm^{-1}.(right). Band assignments are given at the top.
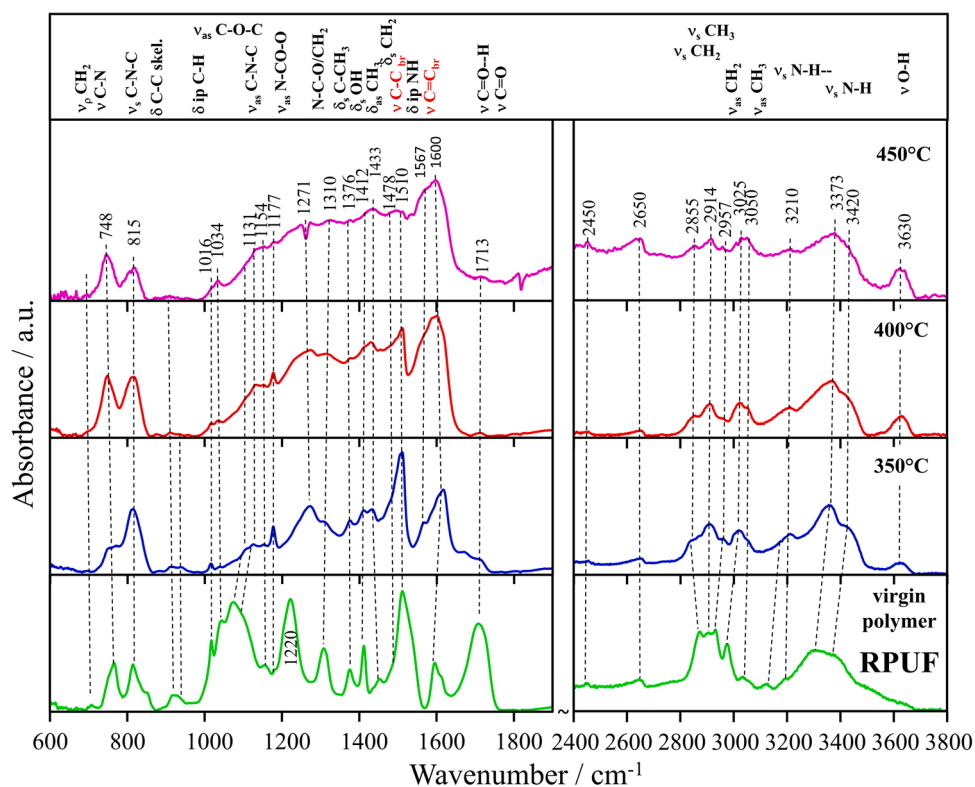
Fig. 4. ATR-FTIR spectra of RPUF and pyrolysis intermediates obtained from segmented thermogravimetric experiments.

of the PUR as per the commonly accepted mechanism.

According to the IR spectra (Fig. 5), FPUF behaves similarly to RPUF. The strongest C-O-C band at 1094 cm^{-1}, typical for the soft segment of FPUF is absent in the spectrum of the 350 °C product. Thus, complete depolymerization and volatilization take place already at lower temperatures. Despite the lower proportion of urethane linkages in the FPUF, in the IR spectra of its intermediate products there are bands of isocyanate derivates at 768 cm^{-1}, 815 cm^{-1} (C-N and C-N-C vibrations) and 1177 cm^{-1}. The C-C and C=C bands typical for skeleton vibrations in the benzene ring (1601 cm^{-1}, 1510 cm^{-1}, 1412 cm^{-1}) are present in the 350 and 400 °C samples. With increasing pyrolysis temperature, the bands at 1510 cm^{-1} and 1601 cm^{-1} gain in intensity, the latter being the strongest band in the spectrum of the 450 °C sample. Therefore, the spectra of the 350 and 400 °C show similarities with MDA as a derivate of MDI. The difference to the behavior of RPUF is that the MDA formed from FPUF seems to be persistent at 400 °C before a partial disintegration takes place at 450 °C. The bands in the high-frequency range behave very similarly to those in the spectra of the RPUF intermediates.

The spectra of the intermediates of CE and TPU samples (Fig. 6 and 7) behave very similarly. The spectra after 350 °C treatment show breakage of the carbonyl urethane bond by disappearing of the bands at 1700 and 1730 cm^{-1}. In addition, the low-frequency bands at 1070 cm^{-1} in the range of C-O-C vibrations are also not present. The band at 1007 cm^{-1} is on the contrary the most intense band in the spectra. Therefore, only a certain part of the polyol segment seems to be not stable at 350 °C. In the CH range, no significant changes are observed. An obvious difference between the 350 °C spectra of CE and TPU on one side and these of RPUF and FPUF on the other is the absence of OH in the former. The spectra after 400 and 450 °C of all samples are strikingly similar, especially those after 450 °C. A reorganization of the CH groups and breakage of the H bonds takes place leading to a frequency shift of the N-H vibrations from 3300 to 3400 cm^{-1}. Stretching OH bands are clearly observed in the spectra of CE and TPU at slightly higher frequencies (3637 cm^{-1}) than these of RPUF and FPUF (3630 cm^{-1}).

For a more general indication of the substance release of the pyrolyzing polymer, elemental analyses of the intermediates were carried out (see Tables SI 1–4 in the supplementary information).

Table 3 shows element mass balances for the intermediates obtained from the segmented TG experiments. For RPUF, in the experiments with an isothermal segment at 350 °C, about 67% of the initial sample mass was converted to volatile products. In the residue, 37% of the original carbon, 27% of the original hydrogen, and 55% of the original nitrogen remain. Thus, a proportionately greater mass of carbon and hydrogen than of nitrogen is expelled. This agrees with the conclusions from the ATR-FTIR investigations. The nitrogen, which is present exclusively in the urethane bond in the polymer under consideration, is incorporated into secondary polymeric structures, or low-volatility products, during the decomposition of the urethanes. Some of these low-volatility nitrogen-bearing intermediates appear to further decompose or evaporate upon increasing the pyrolysis temperature, as the samples obtained at 400 °C and 450 °C contain less nitrogen, at 34% and 25% of the initial mass, respectively. Nevertheless, the proportion of retained nitrogen is large here, so it can be assumed that the isocyanates regenerated from depolymerization, their amine derivatives, and intermediates formed from these are essentially involved in the residue formation. FPUF shows similar behavior in this respect. In the 400 °C and 450 °C intermediates, 41% and 32% of the nitrogen originally contained in the sample is still bound.

Ravey and Pearce [13] and Woolley [47] report an almost quantitative release of the nitrogen contained in flexible PUR foam in the form of the toluene diisocyanate used into the gas phase. This is not the case with the MDI-based FPUF investigated in this work. Lattimer et al. [48] found that during pyrolysis of MDI-polyether-based PUR, cyclic urethane oligomers are formed, which decompose at 325 °C. The remaining nitrogen is in the form of MDA. Guo et al. [12] report large quantities of nitrogen bound in heterocyclic compounds, nitriles, and aromatic amines with aniline, p-aminotoluene, and 4-[(4-aminophenyl)methyl] aniline as the main compounds. These results fit the phenomena observed in this work. The hydrogen contained in the virgin polymer is
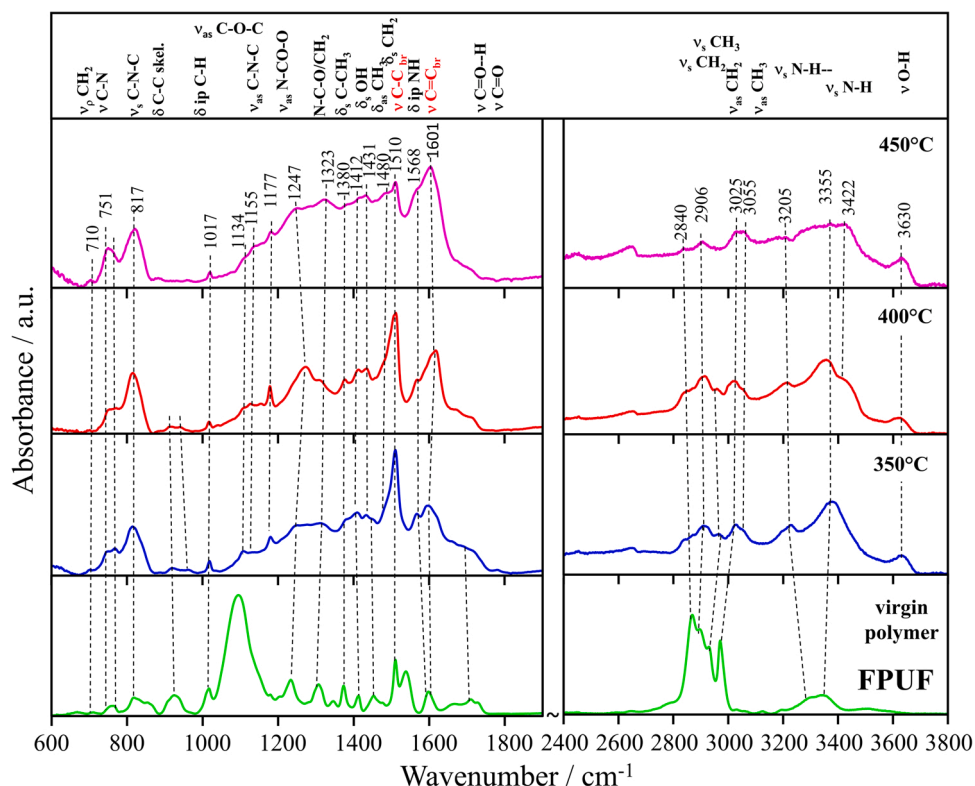
Fig. 5. ATR-FTIR spectra of FPUF and pyrolysis intermediates obtained from segmented thermogravimetric experiments.

Table 3
Elemental Mass Balance of pyrolysis intermediates obtained from segmented TGA experiments.

Sample	Residual Mass	Residual C	Residual H	Molar H/C Ratio	Residual N
	Wt.-%	Wt.-%	Wt.-%	-	Wt.-%
RPUF					
Virgin Polymer	100	100	100	1.2	100
350 °C Intermediate	33	37	27	0.8	55
400 °C Intermediate	21	25	13	0.6	34
450 °C Intermediate	17	19	9	0.5	25
FPUF					
Virgin Polymer	100	100	100	1.5	100
350 °C Intermediate	14	16	8	0.8	48
400 °C Intermediate	12	13	6	0.7	41
450 °C Intermediate	10	11	4	0.6	32
CE					
Virgin Polymer	100	100	100	1.6	100
350 °C Intermediate	18	19	17	1.4	12
400 °C Intermediate	4	5	2	0.6	2
450 °C Intermediate	3	4	1	0.5	1
TPU					
Virgin Polymer	100	100	100	1.4	100
350 °C Intermediate	23	25	23	1.3	14
400 °C Intermediate	7	7	3	0.7	9
450 °C Intermediate	5	6	2	0.5	2

almost completely expelled at 450 °C. The H/C molar ratio shifts from well above 1 in the virgin polymers to about 0.5 in the pyrolysis intermediates at 450 °C. This also reveals residue formation due to double bond formation and cyclization of the pyrolyzing polymer.

The two PTHF-based PUR TPU and CE do not form any significant amount of residue in dynamic, as well as in segmented experiments, and pyrolyze almost completely already at 450 °C. Lattimer et al. [48] observed no formation of cyclic polyethers as pyrolysis products in experiments with PUR based on MDI and PTHF, which is thus similar to the CE and TPU considered in this work. MDI/PTHF-based PUR elastomers studied by Nishiyama et al. [17] also decomposed without significant residue formation in the TGA. They suggest three temperature-dependent pyrolysis stages, in which hard (urethane) and soft segments (PTHF) decompose independently. This suggested behavior is confirmed by our findings.

The effect of nitrogen retention evident in the foams is not observed for CE and TPU. Accordingly, there appears to be no incorporation of the nitrogen-bearing compounds from the depolymerization into the residue. This may be related to the chain structure of the polymers. While cross-links are formed in the foams, long, linear chains are present in CE and TPU. One factor here is the use of the blowing agent water in the production of the foams. Water leads to a change in the molecular structure since ureas and biurets are formed in addition to urethane bonds, which crosslink the chains. Released pyrolysis products from the urethane bonds bind as reaction partners to the existing cross-links and form more temperature-stable oligomers and consequently coke. In the unfoamed PUR TPU and CE, there are little to no cross-links, which is why the evaporation of the pyrolysis products plays a greater role than secondary polymerization and coking.

The foams are based on ethylene oxide and propylene oxide polyether polyols, respectively, while PTHF is used for CE and TPU. The coking behavior of the pure, unpolymerized polyols was investigated in

the TGA, where no char formation was observed (see Figure SI 1 in the supplementary information). This is a further indication that the residue formation primarily and initially originates from the decomposing hard segments.

3.3. Py-GC/MS-Screening

Thermogravimetry and solids analyses described in the previous sections provide good insights into the decomposition behavior of PUR but supply little information about the gaseous and condensable phases of the product spectrum. The aim of the screening investigations presented here was to obtain an overview of the volatile pyrolysis products to complement the aforementioned analyses. Comprehensive and especially quantitative analyses of the product spectrum of PUR require advanced method development. In contrast to TGA, Py-GC/MS as performed here is quasi-isothermal, which results in an overlapped decomposition of the hard and soft segments of the PUR. A pyrolysis temperature of 600 °C was chosen to lower the risk of tar deposition in the system. Fig. 6 and 7.

The pyrograms shown in Fig. 8 reveal characteristic volatile products generated during pyrolysis of the investigated PUR. Various gaseous and highly volatile products eluting in the first minutes of the analysis cannot be separated satisfactorily by the employed GC method. For this reason, the pyrograms were cut to show retention times from 3 to 180 min. Peak intensities were normalized with respect to the highest peak in each pyrogram.

In the case of RPUF, 4,4′-MDA is detected, indicating urethane degradation via 6-membered ring transition [16,17,19] and matching the findings from the ATR-FTIR analyses of the pyrolysis intermediates. A pronounced peak of N,N-dimethyl-cyclohexaneamine is to be noted. This substance was added as a catalyst during sample production and is thus not to be considered a decomposition product of the PUR. Beyond that, p-aminotoluene occurs as a typical product of PUR degradation [12,18,49,50]. Other substances with high abundances, namely dipropylene glycol, propylene glycol, and 1-hydroxy-2-propanone are to be attributed to the soft segment degradation.

The pyrogram of FPUF shows similar compounds to RPUF with 4,4′-MDA, o-aminotoluene and aniline, which hints to equivalent decomposition mechanisms. Plenty of oxygenated compounds with short retention times are detected, which result from the soft segment degradation.

The most abundant peak in the pyrogram of TPU is that of 4,4′-MDI. The presence of 1,4-BDO points to depolymerization of the urethane groups according to 4-membered ring transfer [19] with little MDI derivatization and hence a low tendency for residue formation. The volatile 1,4-BDO generated from this depolymerization gives reason to the intense primary mass loss observed in thermogravimetry. The degradation of the PTHF-based soft segments yields THF and similar compounds.

In relation to the other investigated samples, comparatively high tar deposition in the pyrolysis chamber was observed for the CE. From the TGA results it is evident, that the pyrolysis products of CE initially volatilize. Vaporized pyrolysis products may subsequently condense at cold spots in the micropyrolyzer and consequently cannot be detected in the MS. The product spectrum is therefore only partially captured in the pyrogram. Nonetheless, the pyrogram of the CE shows a large number of peaks, very few of which can be assigned to a compound with a satisfactory match quality. The products of the soft segment decomposition are almost identical to those of TPU. It is striking that none of the typical nitrogen-bearing compounds can be detected. 1,4-BDO is released, which suggests the 4-ring transfer mechanism also found in TPU pyrolysis. However, the likewise expected isocyanate is completely absent. The typical isocyanate decomposition products, MDA, aminotoluene, and aniline, are also not detectable. Despite the same reactants, the polymer structure of CE is different from that of the TPU. A higher fraction of MDI is bound to the long-chained PTHF than to the chain
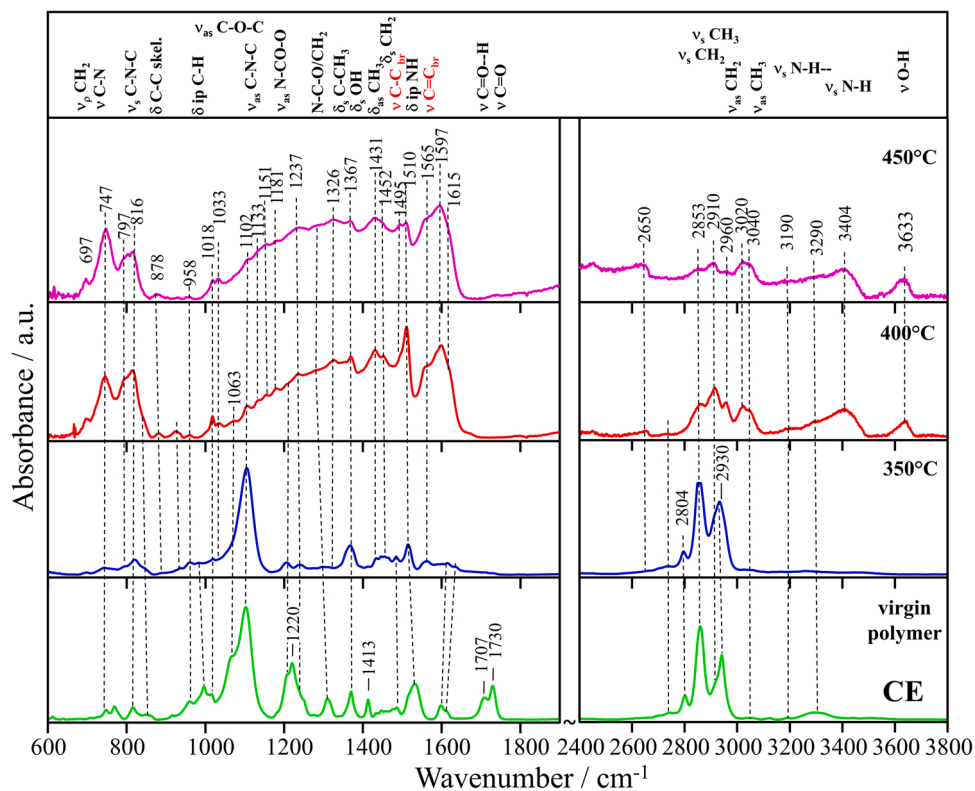
Fig. 6. ATR-FTIR spectra of CE and pyrolysis intermediates obtained from segmented thermogravimetric experiments.
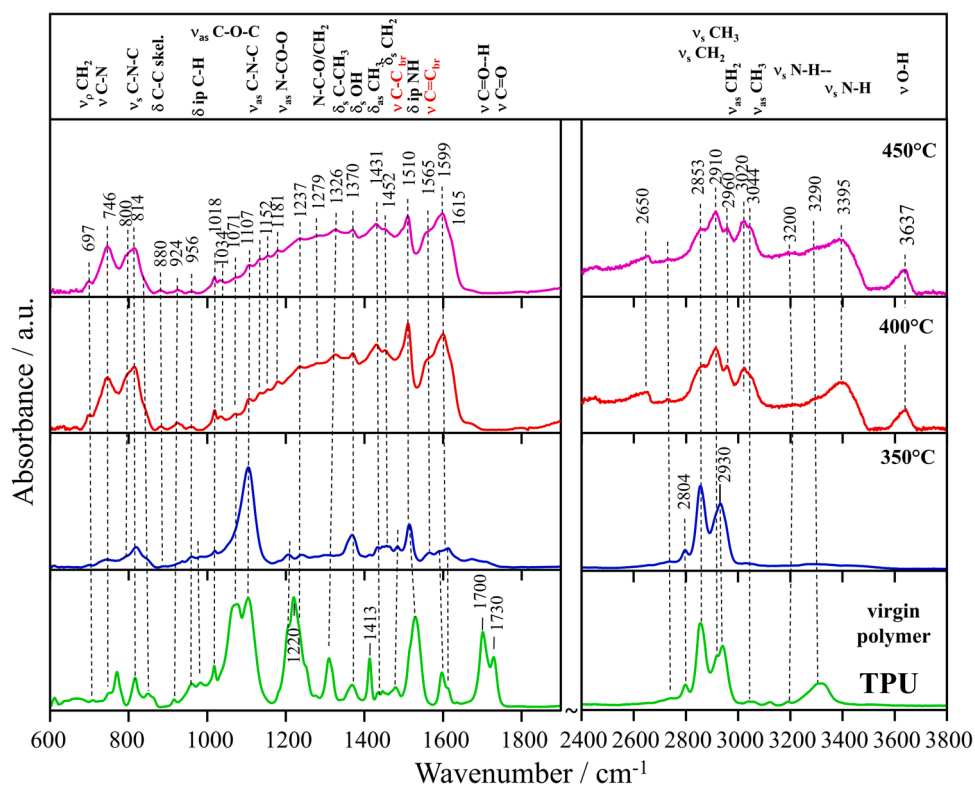
Fig. 7. ATR-FTIR spectra of TPU and pyrolysis intermediates obtained from segmented thermogravimetric experiments.

extender 1,4-BDO. One might assume that the simultaneous degradation of the PTHF and the urethane segments yields oligomers that are prone to condense in cold spots. According to Nishiyama et al. [17] urethane

hard segments consisting of MDI and 1,4-BDO decompose at lower temperatures and yield different products than urethane bonds linking soft segments. This may explain the deviation in the product spectra
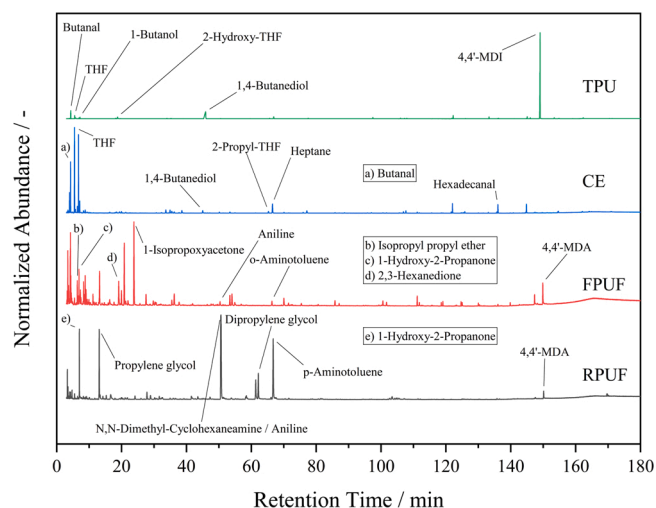
Fig. 8. Pyrograms obtained from Py-GC/MS at a pyrolysis temperature of 600 °C held for 1 min.

presented here.

A manifold of lower-intensity peaks is observed for all PUR samples, indicating a very broad spectrum of further degradation products. Mass spectra obtained for these peaks point to oxygenated products attributable to the soft segments but are not unambiguous. The product spectrum can be resolved more accurately by advanced 2-dimensional gas chromatography, as demonstrated by Eschenbacher et al. [51].

3.4. Kinetic Modeling

In the literature, two pseudo-reactions are usually assumed to describe the pyrolytic degradation of PUR. To find kinetic parameters that describe the decomposition behavior of the investigated PUR as accurately as possible, the IPRM and the CRM were applied. The identified parameters are shown in Table 4. A deviation of the parameter sets of the two models is noticeable, which we attribute to the differences in the model functions. Our results lie well within the range of kinetic parameters reported in the literature [10,11,16,30,50,52–54].

As shown in Fig. 9, both models reproduce the experimental data of all PUR well. Coefficients of determination (R^2) and root mean square errors (RMSE) calculated from experimental data and the respective kinetic models are given in Table 5. The experiments used for validation were conducted with a heating rate of 15 K/min and experimental conditions identical to the experiments used for the parameter

optimization, following the methodology described in Section 2.2.1.

The R^2 values close to unity indicate the high accuracy of both models. The IPRM slightly outperforms the CRM in terms of fit quality. This is also reflected in the RMSE. Values for the IPRM range between 0.011 and 0.017 and are thus lower than CRM RMSE between 0.025 and 0.039.

4. Conclusion

In this work, four different model PUR were investigated by thermogravimetry, Py-GC/MS, and ATR-FTIR. Analyses of the pyrolysis intermediates obtained from TG experiments with isothermal segments with water-blown FPUF and RPUF reveal retention of isocyanate derivates and large fractions of feedstock nitrogen in the form of amines. In intermediates formed in pyrolysis of CE and TPU, little residue formation, and little nitrogen retention were observed. This is attributed to the weakly crosslinked structure, lesser amount of urethane bonds, and absence of blowing agent water.

Py-GC/MS-Analyses show a manifold of degradation products. 1,4-BDO and MDI detected in the product spectrum of TPU indicate depolymerization and evaporation with little derivatization, matching the findings from thermogravimetry and IR spectroscopy. For both TPU and CE, the soft segments consisting of PTHF decompose into various oxygenated products derived from THF. The pyrograms of the PUR foams show MDA and fragments of MDI such as aniline and aminotoluene, pointing to a different degradation route as also evidenced by the IR spectra of the pyrolysis intermediates.

Despite the differences in the pyrolysis products, a two-step degradation mechanism, highly dependent on the PUR structure was confirmed for all materials. Two kinetic modeling approaches based on independent parallel reactions and consecutive reactions respectively were successfully applied for the description of the pyrolytic conversion of the investigated PUR. The distinct two-step degradation behavior of all investigated polymers is reproduced well by both models. In sum, a clearer picture emerges of how PUR compositions and properties correlate with the pyrolysis characteristics and the product spectrum. ATR-FTIR has proven a valuable tool for assessing PUR in this regard.

Future work should focus on PUR-pyrolysis on a scale larger than Py-GC/MS and TGA to characterize the influence of secondary reactions on the product yield and spectrum. The amendment of existing kinetic models to resolve the release of specific products or product groups requires further clarification of the exact products generated during pyrolysis. Both are necessary to develop optimal design parameters for technical PUR pyrolysis to maximize product yield and quality. It is evident that these depend on the PUR type and morphology.

CRediT authorship contribution statement

Michael Zeller: Conceptualization, Methodology, Investigation, Data curation, Formal analysis, Writing – original draft, Visualization. **Krassimir Garbev**: Investigation, Resources, Data curation, Formal analysis, Writing – review & editing, Visualization. **Luca Weige**l: Software, Formal analysis, Data curation, Writing – review & editing. **Tilman Saatzer:** Software, Formal analysis, Data curation. **Daniela Merz**: Methodology, Resources, Writing – review & editing, Supervision. **Salar Tavakkol**: Writing – review & editing, Supervision. **Dieter Stapf**: Writing – review & editing, Supervision, Funding acquisition.

Declaration of Competing Interest

The authors declare the following financial interests/personal relationships which may be considered as potential competing interests: Michael Zeller reports equipment, drugs, or supplies was provided by BASF Polyurethanes GmbH.

Table 4
Optimized kinetic parameters for pyrolysis of PUR.

Sample	Model	Reaction	$v_{i,\infty}$	q_i	$k_{0,i}$	$E_{A,i}$	n
-		-	-	-	1/s	kJ/mol	-
RPUF	IPRM	1	-	0.70	$5.68 \cdot 10^{12}$	174	1.52
		2	-	0.29	$3.58 \cdot 10^{10}$	179	2.08
	CRM	1	0.65	-	$9.37 \cdot 10^{12}$	175	2.05
		2	0.21	-	$6.41 \cdot 10^{14}$	238	2.37
FPUF	IPRM	1	-	0.07	$3.75 \cdot 10^{11}$	152	0.97
		2	-	0.91	$1.05 \cdot 10^{13}$	191	0.97
	CRM	1	0.1	-	$4.92 \cdot 10^{13}$	171	2.86
		2	0.83	-	$1.26 \cdot 10^{14}$	203	1.5
CE	IPRM	1	-	0.18	$1,15 \cdot 10^{11}$	157	0.97
		2	-	0.82	$9.08 \cdot 10^{12}$	198	0.97
	CRM	1	0.21	-	$9.23 \cdot 10^{12}$	178	1.22
		2	0.76	-	$6.24 \cdot 10^{14}$	223	1.16
TPU	IPRM	1	-	0.41	$5.82 \cdot 10^{11}$	166	0.97
		2	-	0.58	$1.75 \cdot 10^{9}$	150	0.96
	CRM	1	0.56	-	$3.42 \cdot 10^{14}$	198	2.51
		2	0.42	-	$1.08 \cdot 10^{14}$	211	1.46

Fig. 9. Experimental and modeled pyrolytic conversion of RPUF (top left), FPUF (top right), CE (bottom left) and TPU (bottom right) at a heating rate of 15 °C/min.

Table 5
Performance indicators for the PUR pyrolysis models.

		RPUF	FPUF	CE	TPU
IPRM	RMSE	0.015	0.017	0.011	0.016
	R^2	0.9989	0.9986	0.9995	0.9988
CRM	RMSE	0.025	0.039	0.037	0.030
	R^2	0.9956	0.9918	0.9935	0.9957

Data Availability

Data will be made available on request.

Appendix A. Supporting information

Supplementary data associated with this article can be found in the online version at doi:10.1016/j.jaap.2023.105976.

References

[1] T. Keijer, V. Bakker, J.C. Slootweg, Circular chemistry to enable a circular economy, Nat. Chem. 11 (2019) 190–195, https://doi.org/10.1038/s41557-019-0226-9.

[2] A. Rahimi, J.M. García, Chemical recycling of waste plastics for new materials production, Nat. Rev. Chem. 1 (2017), https://doi.org/10.1038/s41570-017-0046.

[3] PlasticsEurope AISBL, Plastics - the Facts 2022, 2022, https://plasticseurope.org/knowledge-hub/plastics-the-facts-2022/, accessed 30 January 2023.

[4] G. Brereton, R.M. Emanuel, R. Lomax, K. Pennington, T. Ryan, H. Tebbe, M. Timm, P. Ware, K. Winkler, T. Yuan, Z. Zhu, N. Adam, G. Avar, H. Blankenheim, W. Friederichs, M. Giersig, E. Weigand, M. Halfmann, F.-W. Wittbecker, D.-R. Larimer, U. Maier, S. Meyer-Ahrens, K.-L. Noble, H.-G. Wussow, Polyurethanes, in: Ullmann's Encyclopedia of Industrial Chemistry, 7th ed., Wiley, Weinheim, Wiley online library, 2003, pp. 1–76.

[5] M.M.Alavi Nikje, Recycling of Polyurethane Wastes, De Gruyter, 2019.

[6] D. Simón, A.M. Borreguero, A. de Lucas, J.F. Rodríguez, Recycling of polyurethanes from laboratory to industry, a journey towards the sustainability, Waste Manag. (N. Y., N. Y.) 76 (2018) 147–171, https://doi.org/10.1016/j.wasman.2018.03.041.

[7] M. Kusenberg, A. Eschenbacher, L. Delva, S. de Meester, E. Delikonstantis, G. D. Stefanidis, K. Ragaert, K.M. van Geem, Towards high-quality petrochemical feedstocks from mixed plastic packaging waste via advanced recycling: The past, present and future, Fuel Process. Technol. 238 (2022), 107474, https://doi.org/10.1016/j.fuproc.2022.107474.

[8] P. Neuner, D. Graf, N. Netsch, M. Zeller, T.-C. Herrmann, D. Stapf, R. Rauch, Chemical conversion of fischer–tropsch waxes and plastic waste pyrolysis condensate to lubricating oil and potential steam cracker feedstocks, Reactions 3 (2022) 352–373, https://doi.org/10.3390/reactions3030026.

[9] M. Zeller, N. Netsch, F. Richter, H. Leibold, D. Stapf, Chemical recycling of mixed plastic wastes by pyrolysis – pilot scale investigations, Chem. Ing. Tech. 93 (2021) 1763–1770, https://doi.org/10.1002/cite.202100102.

[10] M.A. Garrido, R. Font, J.A. Conesa, Kinetic study and thermal decomposition behavior of viscoelastic memory foam, Energy Convers. Manag. 119 (2016) 327–337, https://doi.org/10.1016/j.enconman.2016.04.048.

[11] M.A. Garrido, R. Font, Pyrolysis and combustion study of flexible polyurethane foam, J. Anal. Appl. Pyrolysis 113 (2015) 202–215, https://doi.org/10.1016/j.jaap.2014.12.017.

[12] X. Guo, L. Wang, L. Zhang, S. Li, J. Hao, Nitrogenous emissions from the catalytic pyrolysis of waste rigid polyurethane foam, J. Anal. Appl. Pyrolysis 108 (2014) 143–150, https://doi.org/10.1016/j.jaap.2014.05.006.

[13] M. Ravey, E.M. Pearce, Flexible polyurethane foam. I. Thermal decomposition of a polyether-based, water-blown commercial type of flexible polyurethane foam, J. Appl. Polym. Sci. 63 (1997) 47–74, https://doi.org/10.1002/(SICI)1097-4628(19970103)63:1%3C47:AID-APP7%3E3.0.CO;2-S.

[14] X. Tang, X. Chen, Y. He, F. Evrendilek, Z. Chen, J. Liu, Co-pyrolytic performances, mechanisms, gases, oils, and chars of textile dyeing sludge and waste shared bike tires under varying conditions, Chem. Eng. J. 428 (2022), 131053, https://doi.org/10.1016/j.cej.2021.131053.

[15] D. Rosu, N. Tudorachi, L. Rosu, Investigations on the thermal stability of a MDI based polyurethane elastomer, J. Anal. Appl. Pyrolysis 89 (2010) 152–158, https://doi.org/10.1016/j.jaap.2010.07.004.

[16] S. Kumagai, S. Motokucho, R. Yabuki, A. Anzai, T. Kameda, A. Watanabe, H. Nakatani, T. Yoshioka, Effects of hard- and soft-segment composition on pyrolysis characteristics of MDI, BD, and PTMG-based polyurethane elastomers, J. Anal. Appl. Pyrolysis 126 (2017) 337–345, https://doi.org/10.1016/j.jaap.2017.05.012.

[17] Y. Nishiyama, S. Kumagai, S. Motokucho, T. Kameda, Y. Saito, A. Watanabe, H. Nakatani, T. Yoshioka, Temperature-dependent pyrolysis behavior of polyurethane elastomers with different hard- and soft-segment compositions, J. Anal. Appl. Pyrolysis 145 (2020), 104754, https://doi.org/10.1016/j.jaap.2019.104754.

[18] J.-J. He, L. Jiang, J.-H. Sun, S. Lo, Thermal degradation study of pure rigid polyurethane in oxidative and non-oxidative atmospheres, J. Anal. Appl. Pyrolysis 120 (2016) 269–283, https://doi.org/10.1016/j.jaap.2016.05.015.

[19] D.K. Chattopadhyay, D.C. Webster, Thermal stability and flame retardancy of polyurethanes, Prog. Polym. Sci. 34 (2009) 1068–1133, https://doi.org/10.1016/j.progpolymsci.2009.06.002.

[20] J. Oenema, H. Liu, N. de Coensel, A. Eschenbacher, R. van de Vijver, J. Weng, L. Li, C. Wang, K.M. van Geem, Review on the pyrolysis products and thermal decomposition mechanisms of polyurethanes, J. Anal. Appl. Pyrolysis 168 (2022), 105723, https://doi.org/10.1016/j.jaap.2022.105723.

[21] K.M. Zia, H.N. Bhatti, I. Ahmad Bhatti, Methods for polyurethane and polyurethane composites, recycling and recovery: a review, React. Funct. Polym. 67 (2007) 675–692, https://doi.org/10.1016/j.reactfunctpolym.2007.05.004.

[22] E.M. Zakharyan, A.L. Maksimov, Pyrolysis of polyurethanes. process features and composition of reaction products, Russ. J. Appl. Chem. 95 (2022) 191–255, https://doi.org/10.1134/S1070427222020033.

[23] A. Anca-Couce, C. Tsekos, S. Retschitzegger, F. Zimbardi, A. Funke, S. Banks, T. Kraia, P. Marques, R. Scharler, W. de Jong, N. Kienzl, Biomass pyrolysis TGA assessment with an international round robin, Fuel 276 (2020), 118002, https://doi.org/10.1016/j.fuel.2020.118002.

[24] Z. Ding, J. Liu, H. Chen, S. Huang, F. Evrendilek, Y. He, L. Zheng, Co-pyrolysis performances, synergistic mechanisms, and products of textile dyeing sludge and medical plastic wastes, Sci. Total Environ. 799 (2021), 149397, https://doi.org/10.1016/j.scitotenv.2021.149397.

[25] Z. Ding, H. Chen, J. Liu, H. Cai, F. Evrendilek, M. Buyukada, Pyrolysis dynamics of two medical plastic wastes: drivers, behaviors, evolved gases, reaction mechanisms, and pathways, J. Hazard. Mater. 402 (2021), 123472, https://doi.org/10.1016/j.jhazmat.2020.123472.

[26] W. Xu, J. Liu, Z. Ding, J. Fu, F. Evrendilek, W. Xie, Y. He, Dynamic pyrolytic reaction mechanisms, pathways, and products of medical masks and infusion tubes, Sci. Total Environ. 842 (2022), 156710, https://doi.org/10.1016/j.scitotenv.2022.156710.

[27] Y. He, X. Chen, X. Tang, S. Chen, F. Evrendilek, T. Chen, W. Dai, J. Liu, Co-combustion dynamics and products of textile dyeing sludge with waste rubber versus polyurethane tires of shared bikes, J. Environ. Chem. Eng. 11 (2023), 109196, https://doi.org/10.1016/j.jece.2022.109196.

[28] J. Fu, X. Wu, J. Liu, F. Evrendilek, T. Chen, W. Xie, W. Xu, Y. He, Co-circularity of spent coffee grounds and polyethylene via co-pyrolysis: characteristics, kinetics, and products, Fuel 337 (2023), 127061, https://doi.org/10.1016/j.fuel.2022.127061.

[29] S. Vyazovkin, A.K. Burnham, J.M. Criado, L.A. Pérez-Maqueda, C. Popescu, N. Sbirrazzuoli, ICTAC Kinetics Committee recommendations for performing kinetic computations on thermal analysis data, Thermochim. Acta 520 (2011) 1–19, https://doi.org/10.1016/j.tca.2011.03.034.

[30] G. Jomaa, P. Goblet, C. Coquelet, V. Morlot, Kinetic modeling of polyurethane pyrolysis using non-isothermal thermogravimetric analysis, Thermochim. Acta 612 (2015) 10–18, https://doi.org/10.1016/j.tca.2015.05.009.

[31] G. Martínez-Narro, N.J. Royston, K.L. Billsborough, A.N. Phan, Kinetic modelling of mixed plastic waste pyrolysis, Chem. Thermodyn. Therm. Anal. 9 (2023), 100105, https://doi.org/10.1016/j.ctta.2023.100105.

[32] The MathWorks, Inc., Global Optimization Toolbox User's Guide, 2022, https://de.mathworks.com/help/pdf_doc/gads/gads.pdf, accessed 3 February 2023.

[33] H.L. Friedman, Kinetics of thermal degradation of char-forming plastics from thermogravimetry. Application to a phenolic plastic, J. Polym. Sci., C. Polym. Symp. 6 (1964) 183–195, https://doi.org/10.1002/polc.5070060121.

[34] D. Allan, J.H. Daly, J.J. Liggat, Oxidative and non-oxidative degradation of a TDI-based polyurethane foam: Volatile product and condensed phase characterisation by FTIR and solid state 13C NMR spectroscopy, Polym. Degrad. Stab. 161 (2019) 57–73, https://doi.org/10.1016/j.polymdegradstab.2018.12.027.

[35] D.Y. Takamoto, M.A. Petrich, Effect of heterogeneous secondary pyrolysis reactions on the thermal decomposition of polyurethane scrap, Ind. Eng. Chem. Res. 33 (1994) 3004–3009, https://doi.org/10.1021/ie00036a015.

[36] Y. He, D. Qiu, Z. Yu, Investigation on the failure behavior and compressive performance of rigid polyurethane foam treated under aerobic/anaerobic high temperature random vibration, Polym. Test. 106 (2022), 107465, https://doi.org/10.1016/j.polymertesting.2021.107465.

[37] C.S. Wong, K.H. Badri, Chemical analyses of palm kernel oil-based polyurethane prepolymer, MSA 03 (2012) 78–86, https://doi.org/10.4236/msa.2012.32012.

[38] C. Defeyt, J. Langenbacher, R. Rivenc, Polyurethane coatings used in twentieth century outdoor painted sculptures. Part I: comparative study of various systems by means of ATR-FTIR spectroscopy, Herit. Sci. 5 (2017), https://doi.org/10.1186/s40494-017-0124-7.

[39] A.M. Kaminski, M.W. Urban, Interfacial studies of crosslinked urethanes: Part II. The effect of humidity on waterborne polyurethanes; a spectroscopic study, J. Coat. Tech. 69 (1997) 113–121, https://doi.org/10.1007/BF02697762.

[40] L.-S. Teo, C.-Y. Chen, J.-F. Kuo, Fourier transform infrared spectroscopy study on effects of temperature on hydrogen bonding in amine-containing polyurethanes and poly(urethane urea)s, Macromolecules 30 (1997) 1793–1799, https://doi.org/10.1021/ma961035f.

[41] M.M. Coleman, D.J. Skrovanek, J. Hu, P.C. Painter, Hydrogen bonding in polymer blends. 1, FTIR Stud. Urethane-Ether. blends, Macromol. 21 (1988) 59–65, https://doi.org/10.1021/ma00179a014.

[42] A. Wang, S.-R. Shao, H.-C. Wu, C.-X. Tian, F. Luo, J.-H. Li, Z. Li, H. Tan, Effect of Fluorocarbon Side Chain on the Microphase Morphology and Rheological Behavior of Thermoplastic Polyurethanes, Chin J Polym Sci. https://doi.org/10.1007/s10118-022-2865-3.

[43] Spectrometric identification of organic compounds, 8th ed., Wiley, Hoboken, NJ, 2015.

[44] S. Duquesne, M. Le Bras, S. Bourbigot, R. Delobel, G. Camino, B. Eling, C. Lindsay, T. Roels, Thermal degradation of polyurethane and polyurethane/expandable graphite coatings, Polym. Degrad. Stab. 74 (2001) 493–499, https://doi.org/10.1016/S0141-3910(01)00177-X.

[45] L. Jiao, H. Xiao, Q. Wang, J. Sun, Thermal degradation characteristics of rigid polyurethane foam and the volatile products analysis with TG-FTIR-MS, Polym. Degrad. Stab. 98 (2013) 2687–2696, https://doi.org/10.1016/j.polymdegradstab.2013.09.032.

[46] K. Bruckmoser, K. Resch, Investigation of ageing mechanisms in thermoplastic polyurethanes by means of IR and Raman spectroscopy, Macromol. Symp. 339 (2014) 70–83, https://doi.org/10.1002/masy.201300140.

[47] W.D. Woolley, Nitrogen-containing products from the thermal decomposition of flexible polyurethane foams, Brit. Poly. J. 4 (1972) 27–43, https://doi.org/10.1002/pi.4980040105.

[48] R.P. Lattimer, R.C. Williams, Low-temperature pyrolysis products from a polyether-based urethane, J. Anal. Appl. Pyrolysis 63 (2002) 85–104, https://doi.org/10.1016/S0165-2370(01)00143-7.

[49] M.A. Garrido, R. Font, J.A. Conesa, Pollutant emissions from the pyrolysis and combustion of viscoelastic memory foam, Sci. Total Environ. 577 (2017) 183–194, https://doi.org/10.1016/j.scitotenv.2016.10.159.

[50] R. Font, A. Fullana, J. Caballero, J. Candela, A. García, Pyrolysis study of polyurethane, J. Anal. Appl. Pyrolysis 58- 59 (2001) 63–77, https://doi.org/10.1016/S0165-2370(00)00138-8.

[51] A. Eschenbacher, R.J. Varghese, J. Weng, K.M. van Geem, Fast pyrolysis of polyurethanes and polyisocyanurate with and without flame retardant: compounds of interest for chemical recycling, J. Anal. Appl. Pyrolysis 160 (2021), 105374, https://doi.org/10.1016/j.jaap.2021.105374.

[52] G. REIN, C. LAUTENBERGER, A. FERNANDEZPELLO, J. TORERO, D. URBAN, Application of genetic algorithms and thermogravimetry to determine the kinetics of polyurethane foam in smoldering combustion, Combust. Flame 146 (2006) 95–108, https://doi.org/10.1016/j.combustflame.2006.04.013.

[53] D.S. Pau, C.M. Fleischmann, M.J. Spearpoint, K.Y. Li, Determination of kinetic properties of polyurethane foam decomposition for pyrolysis modelling, J. Fire Sci. 31 (2013) 356–384, https://doi.org/10.1177/0734904113475858.

[54] F.E. Rogers, T.J. Ohlemiller, Pyrolysis kinetics of a polyurethane foam by thermogravimetry; a general kinetic method, J. Macromol. Sci.: Part A - Chem. 15 (1981) 169–185, https://doi.org/10.1080/00222338108066438.